Nonlinear response of the Antarctic ice sheet to Quaternary sea level and climate forcing

Michelle Tigchelaar[1], Axel Timmermann[2,3], Tobias Friedrich[4], Malte Heinemann[5], and David Pollard[6]

[1]Center for Ocean Solutions, Stanford University, Palo Alto, CA, USA
[2]Center for Climate Physics, Institute for Basic Science, Busan, South Korea
[3]Pusan National University, Busan, South Korea
[4]Department of Oceanography, University of Hawaiʻi at Mānoa, Honolulu, HI, USA
[5]Institute of Geosciences, Kiel University, Kiel, Germany
[6]Earth and Environmental Systems Institute, Pennsylvania State University, University Park, PA, USA

Correspondence to: M. Tigchelaar (mtigch@stanford.edu)

Abstract. Antarctic ice volume has varied substantially during the Quaternary, with reconstructions suggesting a glacial ice sheet extending to the continental shelf break, and interglacial sea level highstands of several meters. Throughout this period, changes in the Antarctic ice sheet were driven by changes in atmospheric and oceanic conditions and global sea level, yet so far, modeling studies have not addressed which of these environmental forcings dominate, and how they interact in the dynamical

5 ice sheet response. Here we force an Antarctic ice sheet model with global sea level reconstructions and transient, spatially explicit boundary conditions from a 408 ka climate model simulation, not only in concert with each other but, for the first time, also separately. We find that together, these forcings drive glacial-interglacial ice volume changes of 12-14 m SLE, in line with reconstructions and previous modeling studies. None of the individual drivers – atmospheric temperature and precipitation, ocean temperatures, sea level – single-handedly explains the full ice sheet response. In fact, the sum of the individual ice

10 volume changes amounts to less than half of the full ice volume response, indicating the existence of strong nonlinearities and forcing synergy. Both sea level and atmospheric forcing are necessary to create full glacial ice sheet growth, whereas the contribution of ocean melt changes is found to be more a function of ice sheet geometry than climatic change. Our results highlight the importance of accurately representing the relative timing of forcings of past ice sheet simulations, and underscore the need for developing coupled climate-ice sheet modeling frameworks that properly capture key feedbacks.

15

1 Introduction

Though mass loss of the Antarctic ice sheet (AIS) has accelerated in recent decades (IMBIE team, 2018), future melt rates in a warming climate remain highly uncertain (Joughin and Alley, 2011; Church et al., 2013; DeConto and Pollard, 2016). Records show that during the Quaternary (i.e., the past 2.6 million years), the AIS contributed to both glacial sea level drops

20 of more than 10 m (Bentley et al., 2014), as well as rapid deglacial sea level rise (Carlson and Clark, 2012) and interglacial sea

level highstands of several meters (Dutton et al., 2015). Throughout this period, Antarctic mass balance changes were driven by a wide spectrum of external forcings – changes in atmospheric temperatures, accumulation rates, oceanic conditions, and sea level (Tigchelaar et al., 2018) – making the Quaternary an interesting test-bed for constraining future AIS behavior. So far however, the relative contributions of these different external drivers of past AIS variability and their synergies have not been

5   quantified. Here we address how different forcing agents interact during the last four glacial cycles using a set of experiments with an Antarctic ice sheet model.

Unlike the Greenland ice sheet, the Antarctic ice sheet has large marine-based margins. The ice shelves surrounding the AIS have a buttressing effect, and therefore play an important role in determining its stability. Disintegration of ice shelves can lead to rapid discharge from and acceleration of the grounded ice sheet, in particular when the bed deepens towards the ice sheet

10 interior (a process referred to as 'marine ice sheet instability') (Schoof, 2007; Joughin and Alley, 2011). The importance of the Antarctic marine margins mean that both the marine and the atmospheric environment contribute to ice volume changes. The accelerated mass loss of Pine Island Glacier over the past few decades for instance, has been attributed to enhanced sub-shelf melting in response to warming oceans and changing ocean circulation (Jacobs et al., 2011; Pritchard et al., 2012). The 2002 collapse of the Larsen B ice shelf on the other hand, is thought to be the result of preconditioning by a warming

15 atmosphere (van den Broeke, 2005). During the glacial cycles of the Late Quaternary, changes in eustatic sea level (Fig. 1C) further impacted Antarctic ice shelves: changes in the ice flux at the grounding line turn grounded ice into floating ice during sea level rise, and floating ice into grounded ice during sea level drops (Schoof, 2007). Previous modeling studies of Quaternary AIS evolution have identified global sea level as an important pacemaker, especially for the West Antarctic ice sheet (WAIS) (Ritz et al., 2001; Huybrechts, 2002; Pollard and DeConto, 2009). Finally, changes in temperature and circulation patterns

20 drive changes in accumulation rates that can affect both the marine margins and interior ice sheet. Future projections of AIS evolution suggest that in a warming world, accumulation rates will increase as a result of increased atmospheric moisture content, leading to growth of in particular the East Antarctic ice sheet (EAIS) (Huybrechts et al., 2004; Frieler et al., 2015; Medley and Thomas, 2019).

Quaternary climate change is ultimately caused by variations in earth's axial tilt and orbit around the sun (Milankovitch,

25 1941), i.e., precession, eccentricity and obliquity (Fig. 1A,B). These lead to changes in incoming solar radiation that cause a global climate and carbon cycle response that make changes in atmospheric greenhouse gas concentrations – primarily CO_2 (Fig. 1C) – an additional driver of long-term climate variability (Shackleton, 2000). Different climate variables respond differently to each of these forcings, resulting in a rich spectrum of Southern Hemisphere climate variability in both reconstructions (e.g., Steig et al., 2000; Gersonde et al., 2005; Cortese et al., 2007; Jouzel et al., 2007; Ho et al., 2012) and simulations (e.g.,

30 Huybers and Denton, 2008; Menviel et al., 2008; Timmermann et al., 2009; He et al., 2013; Timmermann et al., 2014). Until now however, Antarctic modeling studies have not considered how these forcings interact in driving ice volume changes. Previous studies have either used heavily parameterized climate forcing (Ritz et al., 2001; Huybrechts, 2002; Pollard and DeConto, 2009) or simplified climate and ice sheet configurations (de Boer et al., 2013; Stap et al., 2014); have focused on equilibrium simulations of specific time periods (Golledge et al., 2012); or applied indexed interpolations of extreme climate

35 states (Maris et al., 2015). All of these studies assume that Southern Hemisphere climate variables vary in pace with either

Antarctic temperature reconstructions (Petit et al., 1999) or the benthic oxygen isotope record (Lisiecki and Raymo, 2005). These modeling studies thus ignore the spatial and temporal heterogeneity of Quaternary climate variability, and preclude a better understanding of how different drivers interact.

The aim of this study is to better understand the individual and combined roles of sea level and climate variability in driving Antarctic ice sheet evolution during the Late Quaternary. To that end we have forced a state-of-the-art Antarctic ice sheet model with spatially-varying and time-evolving atmospheric temperature, precipitation and ocean temperature fields from a climate model simulation over the last four glacial cycles, as well as changes in eustatic sea level from Northern Hemisphere ice sheets. This work builds on Tigchelaar et al. (2018), which used a similar modeling setup but did not isolate individual drivers. We conduct a number of sensitivity experiments to explore the separate role and synergy of individual forcings and mechanisms contributing to past ice sheet variability. Looking at individual forcings allows us to identify which are important, which need modeling improvement, and how they might interact nonlinearly in future Antarctic change. Section 2 provides a detailed overview of our climate and ice sheet modeling setup. In Sect. 3 the main results are presented, with Sect. 3.1 discussing Quaternary climate variability, Sect. 3.2 and 3.3 describing the ice sheet response to all and individual drivers, and Sect. 3.4 discussing the responsible mechanisms. Sect. 4 summarizes our results and discusses their implications.

2 Methods

The Late Quaternary orbital and greenhouse gas forcing shown in Fig. 1 is used to drive a transient simulation with an Earth system model of intermediate complexity (EMIC) over the last four glacial cycles (Sect. 2.1). Climate anomalies from this simulation, together with time-varying global sea level (Fig. 1c), are then used as boundary conditions for various sensitivity experiments (Sect. 2.2.3) with the Penn State University ice sheet model (PSU-ISM; Sect. 2.2.1) according to the equations outlined in Sect. 2.2.2. Figure 2 shows a schematic illustration of this modeling setup.

2.1 Climate model

Our ice sheet model experiments are driven with transient climate anomalies spanning the last four glacial cycles (408 ka to present) (Timmermann et al., 2014; Friedrich et al., 2016; Timmermann and Friedrich, 2016), derived from a simulation with the EMIC LOVECLIM (Goosse et al., 2010), which consists of coupled atmospheric, ocean-sea ice and vegetation components. The atmospheric component of LOVECLIM, ECBILT, is a spectral T21 ($\sim 5.625° \times 5.625°$), three-level model based on the quasi-geostrophic equations, extended by estimates of the ageostrophic terms (Opsteegh et al., 1998). The model contains a full hydrological cycle and includes physical parameterizations of diabatic processes (radiative fluxes, sensible and latent heat fluxes) in the thermodynamic equation.

CLIO, the ocean sea-ice component, is a $3° \times 3°$ primitive equation ocean general circulation model with twenty vertical levels, coupled to a thermodynamic-dynamic sea ice model (Goosse and Fichefet, 1999). It uses parameterizations to compute mixing along isopycnals, the effect of mesoscale eddies on diapycnal transport and downsloping currents at the bottom of continental shelves. Finally VECODE is a terrestrial vegetation model that consists of two plant functional types and non-

vegetated desert zones (Brovkin et al., 1997). Each grid cell is assumed to be partially covered by these three land cover types, based on annual mean temperature and rainfall amount and variability.

For the transient climate model simulation, LOVECLIM was forced with time-evolving orbital parameters (Berger, 1978) and reconstructed atmospheric greenhouse gas concentrations (CO_2, CH_4 and N_2O) (Lüthi et al., 2008). The corresponding

5   orbital forcing, annual mean and seasonal insolation changes and CO_2 time series are shown in Fig. 1. In addition, Northern Hemisphere ice sheet conditions were obtained from a transient experiment conducted with the Climate and Biosphere Model, version 2 (CLIMBER-2), coupled to the Northern Hemisphere Simulation Code for Polythermal Ice Sheets (SICOPOLIS) ice sheet model (Ganopolski and Calov, 2011). Orography, albedo and ice mask variations from this simulation are interpolated onto the LOVECLIM grid, where in the presence of land ice, the grid point albedo is set to 0.7 and the vegetation mask is

10   modified. The orography, albedo and ice mask of the Antarctic ice sheet remain constant throughout the simulation. Similarly, time-evolving Antarctic melt water fluxes are not fed back into LOVECLIM. The implications of this lack of ice sheet-climate coupling will be explored in the Discussion.

The orbital, greenhouse gas and ice sheet conditions are applied with a boundary acceleration factor of five (Timm and Timmermann, 2007; Timmermann et al., 2014). The acceleration technique is based on the assumption of relatively fast equili-

15   bration of surface variables to slow external drivers; it thus mostly affects the representation of deep ocean currents (Timm and Timmermann, 2007), but not of surface and thermocline processes that matter for our experiments. This means that 200 model years correspond to 1000 calendar years. The LOVECLIM simulation is conducted using Last Glacial Maximum (LGM) ocean bathymetry (Roche et al., 2007) in order to avoid the internally generated Atlantic meridional overturning circulation oscillations described in Friedrich et al. (2010). While the climate model run follows closely the methodology of Timmermann et al.

20   (2014), in the current simulation the longwave radiative effect of CO_2 was amplified by a factor of 1.97, based on model-proxy comparisons using 63 globally-distributed SST-reconstructions (Friedrich et al., 2016). The resulting net climate sensitivity amounts to $\sim$4 °C per CO_2 doubling (Timmermann and Friedrich, 2016) and yields a more realistic glacial-interglacial amplitude in surface temperatures compared to paleo-proxy data. Our climate modeling strategy is illustrated in the top half of Fig. 2.

25   ## 2.2 Ice sheet model

The 408 ka climate anomalies from LOVECLIM are used to force a number of sensitivity experiments with the PSU-ISM (Fig. 2; Pollard and DeConto, 2009, 2012a; DeConto and Pollard, 2016; Pollard et al., 2016). This model is based on a combination of the scaled shallow ice and shallow shelf approximations, and calculates ice velocity across the grounding line using an ice flux parameterization (Schoof, 2007). Basal sliding on unfrozen beds is calculated using a standard drag law,

30   with the basal sliding coefficients derived from a simple inverse method (Pollard and DeConto, 2012b). Bedrock deformation is modeled as an elastic lithospheric plate above local isostatic relaxation; the equilibrium bedrock and ice-load state is taken to be modern observed (Bedmap2; Fretwell et al., 2013). The model includes vertical diffusion of heat and storage in bedrock below the ice, which is heated from below by a uniform geothermal heat flux for the EAIS and WAIS (Pollard and DeConto, 2012a). The model is discretized on a polar stereographic grid, which for our long sensitivity experiments has a 40 km resolution.

2.2.1 Present-day climate forcing

For modern climate, surface input fields are obtained from the ALBMAP v1 database at 5 km resolution (Le Brocq et al., 2010).
First, annual mean atmospheric temperature T_a^{obs} (Fig. 3a; van de Berg et al., 2006) and accumulation P^{obs} (Fig. 3b; Comiso,
2000) are interpolated onto the ice model grid. Then a lapse rate correction of $\gamma = 0.008\ °C\,m^{-1}$ is applied to the atmospheric

5   temperature to correct for differences between observed (z^{obs}; Le Brocq et al., 2010) and model (z) surface elevation. The
seasonal cycle in atmospheric temperature is parameterized as a sinusoidal cycle with a range of 20 °C at sea level, increasing
linearly with elevation to 30 °C at 3000 m and above (Pollard and DeConto, 2012a), giving $T_a^{obs}(\tau)$. Surface melt rates are
calculated using a positive degree-day (PDD) scheme (Reeh, 1991) that uses different coefficients for ice ($8\ kg\,m^{-2}\,°C^{-1}$) and
snow ($3\ kg\,m^{-2}\,°C^{-1}$) and allows for seasonal refreezing as well as diurnal and synoptic variability (Pollard and DeConto,

10   2012a). Present-day accumulation rates in the model do not contain a seasonal cycle, but are split into rain and snow based on
monthly temperatures.

  While in reality melting at the ice shelf-ocean interface is a function of ocean temperature, salinity and circulation in the ice
shelf cavity (Jacobs et al., 1992), most ice sheet models used for long-term simulations make use of parameterizations based
on sub-surface ocean temperatures alone. This ice model follows the parameterization developed by Martin et al. (2011) for the

15   PISM-PIK model, where oceanic melt is a function of the difference between ocean temperature and the depth-varying freezing
temperature of ocean water. Unlike in Martin et al. (2011), the melt rate dependency on this temperature difference is quadratic
(Holland et al., 2008; Pollard and DeConto, 2012a). For modern conditions, the model interpolates annual mean 400 m-depth
ocean temperatures T_o^{obs} from the World Ocean Atlas (Locarnini et al., 2010) onto the ice sheet model grid (Fig. 3c). In areas
outside the range of the Locarnini et al. (2010) dataset, ocean temperatures are propagated underneath the ice shelves using

20   a nearest neighbor interpolation. In addition, melt rates at vertical ice faces in direct contact with the ocean are calculated by
multiplying the area of each vertical face with the oceanic melt rates at that grid point. Calving rates at the ice shelf edge
are parameterized based on the large-scale stress field, represented by the horizontal divergence of the ice shelf (Pollard and
DeConto, 2012a; Nick et al., 2013). In recent years a new set of parameterizations was introduced to the ice sheet model
representing sub-grid scale processes that have been hypothesized to significantly increase the sensitivity of the Antarctic ice

25   sheet to climatic forcing (Pollard et al., 2015). These parameterizations include increased calving due to hydrofracturing by
surface melt and rainfall draining into crevasses (Nick et al., 2013), as well as structural failure at the grounding line when
the vertical face of ice cliffs is too tall ('cliff failure') (Bassis and Walker, 2012). Combined, these two mechanisms have the
potential to significantly reduce ice shelf extent and buttressing in warm climates (DeConto and Pollard, 2016; Bell et al.,
2018).

30   The mass balance terms in this study are calculated from a file written at run time that stores accumulation (snow+rain),
ablation (abl), oceanic melt (ocn), melting at vertical ocean faces (face) and calving (calv), averaged over the entire ice sheet
area. The ablation term (abl) here represents the combined contributions of evaporation at the surface, melting at the base of
the grounded ice sheet, and percolation of rain, surface melt water and frictional melt water to the base of the ice sheet, minus

refreezing in the ice column. Evaporation and basal melting of grounded ice are both very minor, and surface melt dominates the percolation term; therefore we refer to the ablation term below as 'surface melt'.

2.2.2 Climate and sea level forcing over the last 408 ka

Instead of parameterizing the paleo-climate forcing of the Late Quaternary, as done in previous studies, we force the Penn State
5 ice sheet model with climate anomalies from the 408 ka transient experiment described in Sect. 2.1 (Tigchelaar et al., 2018). The climate anomalies are calculated with respect to the LOVECLIM climatology over the last 200 model years (representing 1000 calendar years) and are bilinearly interpolated to the ice sheet model grid, then applied and updated every 1000 ice sheet model years. For atmospheric temperature T_a, a lapse rate correction of $\gamma = 0.008\ ^\circ\mathrm{C\,m^{-1}}$ is applied to correct for differences between LOVECLIM orography z^{LC} and present-day Antarctic elevation (z^{obs}; Le Brocq et al., 2010), in addition to differences
10 between present-day elevation and elevation at time t ($z(t)$). Subsequently, monthly temperature anomalies are added to the present-day temperature field (Fig. 3a; Sect. 2.2.1):

$$
\begin{aligned}
T_a(t,\tau) = {}& T_a^{\mathrm{obs}}(\tau) - \gamma \times \left(z(t) - z^{\mathrm{obs}} \right) \\
& + \left(T_a^{\mathrm{LC}}(t,\tau) - T_a^{\mathrm{LC}}(0,\tau) \right) + \gamma \times \left(z^{\mathrm{LC}} - z^{\mathrm{obs}} \right),
\end{aligned}
\tag{1}
$$

where t indicates time in years, τ represents month of year, γ is the lapse rate and superscripts 'obs' and 'LC' indicate present-
15 day and LOVECLIM climatologies respectively.

Because the ice sheet model does not include a seasonal cycle for present-day precipitation, precipitation anomalies are calculated with respect to annual mean precipitation. Instead of adding the anomalies to the present-day field, as done for atmospheric temperature, present-day precipitation (P^{obs}) is multiplied with the ratio of monthly LOVECLIM precipitation at time t ($P^{\mathrm{LC}}(t,\tau)$) to present-day LOVECLIM precipitation ($P^{\mathrm{LC}}(0)$):

$$
20 \quad P(t,\tau) = P^{\mathrm{obs}} \times \left(\frac{P^{\mathrm{LC}}(t,\tau)}{P^{\mathrm{LC}}(0)} \right).
\tag{2}
$$

This is done to ensure that precipitation rates do not go below zero. Annual mean ocean temperature anomalies from the 400 m depth level in LOVECLIM are added to the ice model field as

$$
T_o(t) = T_o^{\mathrm{obs}} + \left(T_o^{\mathrm{LC}}(t) - T_o^{\mathrm{LC}}(0) \right).
\tag{3}
$$

The ocean temperature is set not to decrease below -2.18 $^\circ$C, which is the freezing temperature of sea water with a salinity of
25 34.5 psu at 400 m depth (Beckmann and Goosse, 2003).

Figures 3d-f show the differences between LOVECLIM and observed present-day climate. Modeled atmospheric temperatures over the Antarctic interior are too high, even when corrected for differences in observed surface elevation and the T21 spectral representation of Antarctic orography in LOVECLIM (Fig. 3d). Present-day Antarctic precipitation is characterized by a temperature-driven low accumulation regime ($<50\ \mathrm{mm\,a^{-1}}$) over the Antarctic interior and much higher precipitation rates
30 in coastal areas ($>1000\ \mathrm{mm\,a^{-1}}$) as a result of cyclonic activity and topographic uplift (Bromwich, 1988). LOVECLIM does not capture the complex coastal topography of Antarctica well, and therefore underestimates coastal precipitation, distributing

it over the ice sheet interior instead (Fig. 3e; Maris et al., 2012). Sub-surface ocean temperatures in LOVECLIM are generally too low in the Southern Ocean, except below the shelves, where they are higher than in the World Ocean Atlas climatology. The lower LOVECLIM temperatures might be related to the fact that for present-day climate, minimum sea ice extent is overestimated (Roche et al., 2012). It should also be noted however that the observed climatology in the Southern Ocean is

5 based on a relatively low number of observations, especially close to the Antarctic continent (Locarnini et al., 2010). In any case, LOVECLIM climate anomalies rather than the full fields are applied to the ice sheet model to avoid the propagation of LOVECLIM biases into the ice sheet evolution. As will be discussed in Sect. 3.1, in spite of present-day biases, LOVECLIM simulates the Quaternary climate evolution well.

In addition to climate anomalies, the ice sheet model is forced with time-evolving sea level. Sea level variations are derived

10 from Spratt and Lisiecki (2016) and are plotted in Fig. 1c. While the climate fields are updated every 1000 years, sea level evolves continuously. The bottom half of Fig. 2 illustrates how the climate anomalies and sea level are used to drive the ice sheet model.

2.2.3 Sensitivity experiments

The main ice sheet model simulation is run for 408 ka and includes all drivers described in Sect. 2.2.2 (experiment 'all').

15 In order to isolate the effects of these individual external forcings on Antarctic ice sheet variability and their interaction, we performed a series of sensitivity experiments that include only one or multiple drivers. The individual drivers are either the atmospheric forcing described by Eqs. (1) and (2), the ocean temperature forcing of Eq. (3) or the sea level variations from Spratt and Lisiecki (2016) (experiments 'atm', 'ocn' and 'sl', respectively). In addition to these singular forcing experiments, the model is forced with combinations of two of these three forcings (experiments 'sl+atm', 'sl+ocn' and 'atm+ocn'). These

20 experiments are designed to quantify the synergistic response of the Antarctic ice sheet to a variety of acting forcings. All sensitivity experiments are summarized in Table 1.

3 Results

3.1 Late Quaternary climate forcing

The spatial and temporal evolution of atmospheric temperature, precipitation and sub-surface ocean temperatures are charac-

25 terized by the first principal component (PC1) and the corresponding spatial pattern (EOF1) as shown in Fig. 3g-l. As can be seen in Fig. 3j, annual mean surface temperatures over Antarctica are predominantly paced by changes in atmospheric CO_2 (Fig. 1c). Timmermann et al. (2014) showed that obliquity also contributes to annual mean temperature changes, by affecting annual mean insolation (Fig. 1b) and modulating the strength of the Southern Hemisphere westerlies. The dominant pattern of annual mean temperature changes is homogeneous, with a glacial-interglacial amplitude of ∼4-8 °C (Fig. 3g). When compared

30 to a composite of temperature reconstructions from ice cores (Parrenin et al., 2013), the temporal evolution of the LOVECLIM PC1 is very similar, but the amplitude is underestimated by a factor of 1.5-2, partially due to the fact that the LOVECLIM

simulation does not include the lapse rate response to the evolving ice sheet height. In addition to annual mean temperatures, surface ablation rates are sensitive to changes in seasonal insolation (Huybers and Denton, 2008; Huybers, 2009; Tigchelaar et al., 2018), which is precessionally driven and shown in Fig. 1b.

Precipitation changes display a temporal evolution very similar to that of the atmospheric temperature PC1 (Fig. 3k), con-
5 firming that temperature is the dominant driver of precipitation over Antarctica. When compared to a composite of ice core accumulation reconstructions (Steig et al., 2000; Bazin et al., 2013; Vallelonga et al., 2013), LOVECLIM is shown to overesti-mate precipitation rates during early glacial times. Steig et al. (2000) describe how when the Antarctic ice sheet is expanding, the coastal ice core locations switch from a cyclonic-driven precipitation regime to one driven by temperature with increasing distance from the ice edge. The local precipitation evolution captured by the ice cores thus differs from the large-scale evolution
10 captured by the principal component analysis. This ice sheet-climate feedback is not included in our LOVECLIM simulations.

The temporal evolution of sub-surface ocean temperatures in LOVECLIM (Fig. 3l) is similar to that of surface (not shown) and atmospheric temperatures (Fig. 3j). To our knowledge no reconstructions of intermediate water temperatures in the South-ern Ocean exist, so we compare against a long sea surface temperature (SST) record from 54 °S (Ho et al., 2012). Both in our model simulation as well as in reconstructions, Southern Ocean SST variability is closely related to changes in sea ice area and
15 production, explaining why there is substantial precessional variability in these time series (Timmermann et al., 2009). The LOVECLIM-simulated ocean temperature anomalies close to the Antarctic continent are very small, with the exception of the Weddell sector. The effect of this possible underestimation of ocean forcing on ice sheet evolution will be discussed further below.

3.2 Ice volume response to external forcing

20 Figure 4 shows the simulated response of Antarctic total, grounded, and floating ice volume to the individual and combined Late Quaternary forcings over the last four glacial cycles. With all forcings combined ('all'), the glacial-interglacial difference in ice volume is $\sim 8 \times 10^6$ km^3, or 12-14 m sea level equivalent (SLE) depending on the glacial stage (Fig. 4). During glacial periods, floating ice volume is reduced by about half the present day value ($\sim 7 \times 10^5$ km^3) (Fig. 4c). In our simulations, previous interglacials only contribute 1-2 m to global sea level ($\sim 1 \times 10^6$ km^3), with the deepest interglacial occurring at
25 210 ka (Termination IIIa). Tigchelaar et al. (2018) showed that local changes in summer insolation play an important role in amplifying interglacial ice loss.

The dominant spatial pattern of ice sheet thickness variability in the 'all' simulation, along with minimum (210 ka) and maximum (18 ka) grounding line extent, are shown in Fig. 5a. At its maximum extent, the grounding line reaches to the continental shelf break everywhere. The simulated minimum grounding line extent over the last 408 ka is very similar to
30 present-day, with further retreat mostly of the Ross and Weddell ice shelves in West Antarctica, and the West and Shackleton ice shelves in East Antarctica. Changes in ice sheet thickness are most pronounced in those regions where the grounded ice sheet expands, in particular the Ross and Weddell sectors, Amundsen Sea and Amery shelf. In the interior of the AIS, thickness changes are generally smaller, but mostly of the same sign.

3.3 Nonlinear response to climate and sea level forcing

Not one of the individual drivers of Quaternary AIS variability – sea level, atmospheric temperature and precipitation, ocean temperatures – single-handedly explains the full ice volume evolution (Fig. 4a). Moreover, all of the individual forcings combined only account for less than half of the total ice volume changes, suggesting that they do not add linearly. The largest

5   contribution in terms of both total and grounded ice volume comes from the atmospheric forcing, which explains about a third of glacial ice volume gain, and the entirety of interglacial ice volume loss (Fig. 4a,b). The case is different for floating ice: here sea level changes are responsible for most of the variability, as a lowering sea level converts floating into grounded ice (Fig. 4c; Schoof, 2007). Interestingly, for the floating ice volume, the sum of the individual simulations is not only smaller than, but also often not of the same sign as the floating ice volume changes in the 'all' simulation. When the ice sheet model is forced with

10   two out of three forcings, sea level and atmospheric forcing together almost entirely explain the changes in both grounded and floating ice volume (Fig. 6).

Figure 5 shows where on the Antarctic continent the individual drivers have the largest effect. The sea level forcing drives expansion of the grounding line in the Amundsen, Ross, and Weddell Sea sectors, with small corresponding elevation changes (Fig. 5b). Atmospheric cooling leads to grounding line expansion primarily in the Amundsen, Weddell, and Amery regions,

15   and also leads to thickening of most of the ice shelves (Fig. 5c). During interglacials, the atmospheric forcing causes retreat primarily of the West and Shackleton ice shelves. The oceanic forcing alone affects Antarctic ice volume only minimally. In fact, the dominant spatial pattern of ice thickness variability for the 'ocn' simulation only explains ∼10% of the variance, and is not driven by external forcing, but rather displays internally generated ice sheet variability in the Siple Dome region (Fig. 5d) with a period of ∼10 ka (not shown).

20   When more than one external forcings are combined, the grounding line is able to expand further than with just the single forcings (Fig. 5e-g). As noted above, sea level and atmospheric forcing combined (Fig. 5e) explain most of the grounding line and elevation changes simulated in the full run (Fig. 5a). A combination of sea level and ocean forcing (Fig. 5f) leads to grounding line expansion and ice sheet growth in the Weddell Sea sector, while atmospheric and ocean forcing combined (Fig. 5g) mostly cause ice sheet growth in the Ross Sea.

3.4 Mechanisms explaining ice volume changes

3.4.1 Sea level forcing

Figure 7 plots changes in grounded and ice volume changes in the different sensitivity runs against their respective forcing functions. Again, it is evident that the role of the sea level forcing in isolation is to directly turn grounded into floating ice (Fig. 7a). The corresponding mass balance changes are shown in Fig. 8. With sea level as the only driver, changes in mass

30   balance rates are a feedback to the changes in ice sheet configuration. Ice-sheet integrated surface melt rates (Fig. 8b) increase during glacial periods of sea level drop, because the edges of the ice sheet – where all surface melt occurs – are lower in elevation, with associated higher temperatures. Calving rates (Fig. 8d) similarly increase during periods of low sea level, because the grounding line is positioned more equator-ward (Fig. 5), increasing ice shelf divergence (Tigchelaar et al., 2018).

On the other hand, ice-sheet integrated oceanic melt rates (Fig. 8c) decrease when sea level drops, because the ice-ocean interface area is reduced. These mass balance feedbacks mostly cancel out in the net mass balance (Fig. 8e), explaining why total ice volume changes under isolated sea level forcing are small (Fig. 4).

3.4.2 Atmospheric forcing

5　When atmospheric forcing is applied in isolation, grounded ice volume fairly consistently increases with decreasing surface temperature, whereas floating ice volume plateaus for ice-sheet averaged temperatures lower than $\sim$-34°C (Fig. 7b). Now, the mass balance response (Fig. 8) is a combination of both forcing and feedback. Surface melt rates (Fig. 8b) most directly follow the climatic forcing. As detailed in Tigchelaar et al. (2018), periods of high CO_2 and high summer insolation (Fig. 1) are marked by peaks in summer melt rates that also drive increases in calving rates (Fig. 8d). During these periods, the AIS

10　retreats to areas that have lower accumulation rates (Fig. 3b), amplifying the forcing. In cold periods, a reduction in surface melt and calving leads to a small expansion of floating ice volume (Fig. 4c), which allows the floating ice shelves to sit in climatologically warmer waters (Fig. 3c), increasing glacial ocean melt rates (Fig. 8c). At the same time, the glacial ice sheet extends to areas of climatologically high snow fall. The changes in calving rates and ocean melt rates largely balance, so that peaks in accumulation rates drive much of the ice sheet growth during glacial periods (Fig. 8e).

15　### 3.4.3　Ocean temperature forcing

Out of the three individual drivers, the ocean temperature forcing by itself leads to the least change in grounded and floating AIS volume, as seen in Figs. 4 and 5d. LOVECLIM-modeled ocean temperature changes are fairly small in amplitude (Fig. 3i), and lead to small increases in grounded and floating ice thickness during glacial periods (Fig. 7c). The accompanying mass balance changes are similarly small (Fig. 8). Glacial expansion of floating ice area (Fig. 4c) brings ice shelves into areas with

20　climatologically higher precipitation rates (Fig. 3b), leading to higher glacial accumulation rates (Fig. 8a). The reduced oceanic melt and increased accumulation are balanced by higher calving rates (Fig. 8d).

3.4.4　Combined forcings

Our sensitivity runs show that the response of the Antarctic ice sheet to Quaternary external drivers is a nonlinear superposition of a) a direct mass balance response to climate variations, b) sea-level induced conversion between grounded and floating ice,

25　and c) areal expansion or contraction against climatological gradients. As shown in Fig. 7d-f, when all forcings combine, sea level is the dominant pace maker of both grounded and floating ice volume. Because sea level and atmospheric temperature vary in concert throughout the Quaternary (Fig. 1c, Fig. 3j), grounded ice volume also increases with lowering temperatures, while floating ice volume now decouples from atmospheric temperatures (Fig. 7e). The joint sea level and atmospheric forcing amplify each other in the total ice volume response, because the combination of shelf-to-sheet conversion (Fig. 4c) and reduced

30　calving rates (Fig. 8d) allow the grounding line to migrate equator-ward during glacial times (Fig. 5). This increases the ice

sheet area – and thus the ice-sheet integrated accumulation rate (Fig. 8a) – leading to a net positive mass balance (Fig. 8e), and ice sheet growth.

With all forcings combined, the ice sheet response is completely decoupled from the oceanic temperature forcing (Fig. 4f). During glacial periods, the grounding line is closer to warmer Circumpolar Deep Water (Fig. 3c), so that periods of high total ice volume are associated with high ocean temperatures beneath the ice shelves. This is also seen in Fig. 8c, where ice-sheet averaged oceanic melt rates in the 'all' simulation more closely follow those of the 'atm' run than the 'ocn' run. The spatial gradients in ocean temperature are thus larger and more important than temporal (glacial-interglacial) temperature variations (Fig. 3). The main exception to this is the Ross sector, where decreasing ocean temperatures allow for further ice expansion and grounding line migration during glacial times (compare e.g., Fig. 5c & g). Though a similar dependence of glacial oceanic melt rates on grounding line position rather than climate forcing was also found by Kusahara et al. (2015), we will briefly discuss the validity of these results below.

4 Discussion & Conclusions

Here we presented results from simulations of Antarctic ice sheet evolution over the past 408 ka. In contrast to previous work which primarily used parameterized forcing, climate anomalies (atmospheric temperature, precipitation and sub-surface ocean temperatures) were directly derived from a transient simulation with the EMIC LOVECLIM. The simulated AIS has a glacial-interglacial amplitude of 12–14 m SLE, with the glacial grounding line extending almost entirely to the continental shelf break, and past interglacials showing limited retreat of 1–2 m SLE. Sensitivity experiments where atmospheric, oceanic and sea level forcing were applied in isolation or in pairs, showed that the combined effect of individual forcings is strongly nonlinear. Each of the individual forcings explains less than a third of the full response, and the sum of the individual forcing simulations is less than half of the glacial-interglacial amplitude with all forcings applied jointly. In our simulations, sea level and atmospheric forcing together explain most of the full response, both in terms of amplitude and pacing.

While during glacial periods the dynamics of a lowering sea level and a cooling climate amplify each other in AIS growth, interglacial ice volume loss is almost entirely driven by climate forcing alone (Fig. 4). Tigchelaar et al. (2018) showed that maximum interglacial ice loss occurs when high CO_2 concentrations coincide with high Southern Hemisphere summer insolation (Fig. 1). These precessionally-forced periods of warm summers are typically out of phase with eustatic sea level forcing, which is predominantly paced by warm Northern Hemisphere summers (Raymo et al., 2006). Our simulations therefore do not fully explore the response of the AIS to combined climate warming and rising sea levels, as they would co-occur in future climate change. So far, modeling studies of future Antarctic ice sheet evolution (e.g., Joughin and Alley, 2011; Scambos et al., 2017; DeConto and Pollard, 2016) have not included changes in eustatic sea level. Further research should therefore explore whether, given the current configuration of grounding line and bedrock (Joughin and Alley, 2011; Joughin et al., 2014), rising sea levels would have the potential to increase ice loss due to warming.

The strongly nonlinear response of the AIS to different external forcing agents also underscores the importance of supplying the ice sheet model with accurately dated sea level and climate forcing. Previous modeling studies of past AIS evolution (Ritz

et al., 2001; Huybrechts, 2002; Pollard and DeConto, 2009) have mostly bypassed this issue by assuming that both the sea level and climate forcing vary in concert with either Antarctic temperature reconstructions or the benthic δ^{18}O record. However, as shown in Fig. 1c, global sea level and global climate (i.e., CO_2) do not always vary entirely in phase. Meanwhile, Tigchelaar et al. (2018) highlighted the importance of local summer insolation in addition to global climate variability. At the same time,

5   there are significant uncertainties in the timescales of especially Antarctic climate and CO_2 reconstructions (Lüthi et al., 2008; Bazin et al., 2013). Repeating the LOVECLIM climate simulations with a proper uncertainty range in atmospheric greenhouse gas concentrations would be computationally unfeasible, though future sensitivity runs with the ice sheet model could manually offset the sea level and climate forcing to explore associated nonlinearities.

Finally, our results clearly highlight the interplay between spatial gradients in Southern Hemisphere climate and the temporal

10 evolution of the Antarctic ice sheet. In particular, as the ice sheet grows, it sits in areas of higher precipitation and warmer ocean water, acting as a positive and negative feedback respectively. However, in this modeling setup we are not able to account for feedbacks between ice sheet configuration and climate. In the case of precipitation, changes in orography and albedo could substantially alter atmospheric circulation patterns and associated rainfall (Steig et al., 2000; Maris et al., 2014; Steig et al., 2015).

15 As for ocean temperatures, the limited direct response of the AIS to ocean temperature changes could be due to the small glacial-interglacial amplitude simulated by LOVECLIM, though a study by Kusahara et al. (2015) with a much more advanced and high-resolution ocean-ice sheet model also found glacial oceanic melt rate changes to respond to ice sheet geometry instead of climatic change. In reality, melting at the ice-ocean interface depends on much more than sub-surface ocean temperatures alone. The blocking effects of sea ice formation (Hellmer et al., 2012), the role of winds in pushing warm waters onto the

20 continental shelf (Thoma et al., 2008; Steig et al., 2012), and the complex geometry of ice shelf cavities (Jacobs et al., 2011; De Rydt et al., 2014) have all been found to be important in observational and modeling studies of current and future oceanic melting of the WAIS ice shelves (Joughin et al., 2014). Additionally, melt water fluxes from the AIS have been found to lead to cooling of surface waters and warming at intermediate depth (Menviel et al., 2010; Weber et al., 2014), a feedback that could increase ice sheet loss (Golledge et al., 2014, 2019). These processes can only be captured in fully coupled ocean-atmosphere-

25 ice sheet simulations at high resolution, something that is currently not feasible for the long timescales of Quaternary climate evolution.

In response to changes in atmospheric and oceanic conditions and global sea level, Antarctic ice volume has varied by tens of m SLE throughout the Quaternary, and is expected to decrease in the future. Previous modeling studies have failed to elucidate how these different external drivers interact in driving large glacial ice sheet growth and interglacial sea level highstands. Our

30 sensitivity experiments with an Antarctic ice sheet model over the last four glacial cycles show that the glacial-interglacial ice sheet response to environmental forcing is strongly nonlinear. Both a transformation of dynamic regime by lowering sea level and atmospheric cooling are necessary to generate full glacial ice sheet growth. Our results suggest that the contribution of future sea level rise to Antarctic ice loss, which has so far remained unexplored, needs to be incorporated in future modeling, while further underscoring the need for coupled climate-ice sheet modeling.

5   *Data availability.* Our ice sheet simulations are publicly available at https://climatedata.ibs.re.kr/grav/data/psu-love/.

Competing interests. The authors declare that they have no conflicts of interest.

References

Bassis, J. N. and Walker, C. C.: Upper and lower limits on the stability of calving glaciers from the yield strength envelope of ice, Proceedings of the Royal Society A, 468, 913–931, 2012.

Bazin, L., Landais, A., Lemieux-Dudon, B., Toyé Mahamadou Kele, H., Veres, D., Parrenin, F., Martinerie, P., Ritz, C., Capron, E., Lipenkov, V., Loutre, M. F., Raynaud, D., Vinther, B., Svensson, A., Rasmussen, S. O., Severi, M., Blunier, T., Leuenberger, M., Fischer, H., Masson-Delmotte, V., Chappellaz, J., and Wolff, E.: An optimized multi-proxy, multi-site Antarctic ice and gas orbital chronology (AICC2012): 120-800 ka, Clim. Past, 9, 1715–1731, 2013.

Beckmann, A. and Goosse, H.: A parameterization of ice shelf-ocean interaction for climate models, Ocean Model., 5, 157–170, 2003.

Bell, R. E., Banwell, A. F., Trusel, L. D., and Kingslake, J.: Antarctic surface hydrology and impacts on ice-sheet mass balance, Nat. Clim. Chang., 8, 1044–1052, 2018.

Bentley, M. J., Ó Cofaigh, C., Anderson, J. B., Conway, H., Davies, B., Graham, A. G. C., Hillenbrand, C.-D., Hodgson, D. a., Jamieson, S. S. R., Larter, R. D., Mackintosh, A., Smith, J. a., Verleyen, E., Ackert, R. P., Bart, P. J., Berg, S., Brunstein, D., Canals, M., Colhoun, E. a., Crosta, X., Dickens, W. a., Domack, E., Dowdeswell, J. a., Dunbar, R., Ehrmann, W., Evans, J., Favier, V., Fink, D., Fogwill, C. J., Glasser, N. F., Gohl, K., Golledge, N. R., Goodwin, I., Gore, D. B., Greenwood, S. L., Hall, B. L., Hall, K., Hedding, D. W., Hein, A. S., Hocking, E. P., Jakobsson, M., Johnson, J. S., Jomelli, V., Jones, R. S., Klages, J. P., Kristoffersen, Y., Kuhn, G., Leventer, A., Licht, K., Lilly, K., Lindow, J., Livingstone, S. J., Massé, G., McGlone, M. S., McKay, R. M., Melles, M., Miura, H., Mulvaney, R., Nel, W., Nitsche, F. O., O'Brien, P. E., Post, A. L., Roberts, S. J., Saunders, K. M., Selkirk, P. M., Simms, A. R., Spiegel, C., Stolldorf, T. D., Sugden, D. E., van der Putten, N., van Ommen, T., Verfaillie, D., Vyverman, W., Wagner, B., White, D. a., Witus, A. E., and Zwartz, D.: A community-based geological reconstruction of Antarctic Ice Sheet deglaciation since the Last Glacial Maximum, Quat. Sci. Rev., pp. 1–9, 2014.

Berger, A. L.: Long-term variations of daily insolation and Quaternary climatic changes, J. Atmos. Sci., 35, 2362–2367, 1978.

Bromwich, D. H.: Snowfall in High Southern Latitudes, Rev. Geophys., 26, 149–168, 1988.

Brovkin, V., Ganopolski, A., and Svirezhev, Y.: A continuous climate-vegetation classification for use in climate-biosphere studies, Ecol. Modell., 101, 251–261, 1997.

Carlson, A. E. and Clark, P. U.: Ice sheet sources of sea level rise and freshwater discharge during the last deglaciation, Rev. Geophys., 50, RG4007, 2012.

Church, J. A., Clark, P. U., Cazenave, A., Gregory, J. M., Jevrejeva, S., Levermann, A., Merrifield, M. A., Milne, G. A., Nerem, R. S., Nunn, P. D., Payne, A. J., Pfeffer, W. T., Stammer, D., and Unnikrishnan, A. S.: Sea level change, in: Climate Change 2013: The Physical Science Basis. Contribution of Working Group I to the Fifth Assessment Report of the Intergovernmental Panel on Climate Change, edited by Stocker, T. F., Qin, D., Plattner, G.-K., Tignor, M., Allen, S. K., Boschung, J., Nauels, A., Xia, Y., Bex, V., and Midgley, P. M., pp. 1137–1216, Cambridge University Press, Cambridge, United Kingdom and New York, NY, USA, 2013.

Comiso, J. C.: Variability and trends in Antarctic surface temperatures from In Situ and satellite infrared measurements, J. Clim., 13, 1674–1696, 2000.

Cortese, G., Abelmann, A., and Gersonde, R.: The last five glacial-interglacial transitions: A high-resolution 450,000-year record from the subantarctic Atlantic, Paleoceanography, 22, 1–14, 2007.

de Boer, B., van de Wal, R. S. W., Lourens, L. J., Bintanja, R., and Reerink, T. J.: A continuous simulation of global ice volume over the past 1 million years with 3-D ice-sheet models, Clim. Dyn., 41, 1365–1384, 2013.

De Rydt, J., Holland, P. R., Dutrieux, P., and Jenkins, A.: Geometric and oceanographic controls on melting beneath Pine Island Glacier, J. Geophys. Res. C: Oceans, 119, 2420–2438, 2014.

DeConto, R. M. and Pollard, D.: Contribution of Antarctica to past and future sea-level rise, Nature, 531, 591–597, 2016.

Dutton, A., Carlson, A. E., Long, A. J., Milne, G. A., Clark, P. U., DeConto, R. M., Horton, B. P., Rahmstorf, S., and Raymo, M. E.: Sea-level
5   rise due to polar ice-sheet mass loss during past warm periods, Science, 349, 153–162, 2015.

Fretwell, P., Pritchard, H. D., Vaughan, D. G., Bamber, J. L., Barrand, N. E., Bell, R., Bianchi, C., Bingham, R. G., Blankenship, D. D., Casassa, G., Catania, G., Callens, D., Conway, H., Cook, a. J., Corr, H. F. J., Damaske, D., Damm, V., Ferraccioli, F., Forsberg, R., Fujita, S., Gim, Y., Gogineni, P., Griggs, J. a., Hindmarsh, R. C. a., Holmlund, P., Holt, J. W., Jacobel, R. W., Jenkins, A., Jokat, W., Jordan, T., King, E. C., Kohler, J., Krabill, W., Riger-Kusk, M., Langley, K. a., Leitchenkov, G., Leuschen, C., Luyendyk, B. P., Matsuoka, K.,
10   Mouginot, J., Nitsche, F. O., Nogi, Y., Nost, O. a., Popov, S. V., Rignot, E., Rippin, D. M., Rivera, A., Roberts, J., Ross, N., Siegert, M. J., Smith, a. M., Steinhage, D., Studinger, M., Sun, B., Tinto, B. K., Welch, B. C., Wilson, D., Young, D. a., Xiangbin, C., and Zirizzotti, A.: Bedmap2: Improved ice bed, surface and thickness datasets for Antarctica, Cryosphere, 7, 375–393, 2013.

Friedrich, T., Timmermann, A., Menviel, L., Timm, O. E., Mouchet, A., and Roche, D. M.: The mechanism behind internally generated centennial-to-millennial scale climate variability in an earth system model of intermediate complexity, Geoscientific Model Development,
15   3, 377–389, 2010.

Friedrich, T., Timmermann, A., Tigchelaar, M., Timm, O. E., and Ganopolski, A.: Nonlinear climate sensitivity and its implications for future greenhouse warming, Science Advances, 2, e1501 923, 2016.

Frieler, K., Clark, P. U., He, F., Buizert, C., Reese, R., Ligtenberg, S. R. M., van den Broeke, M. R., Winkelmann, R., and Levermann, A.: Consistent evidence of increasing Antarctic accumulation with warming, Nat. Clim. Chang., 5, 348–352, 2015.

20   Ganopolski, A. and Calov, R.: The role of orbital forcing, carbon dioxide and regolith in 100 kyr glacial cycles, Clim. Past, 7, 1415–1425, 2011.

Gersonde, R., Crosta, X., Abelmann, A., and Armand, L.: Sea-surface temperature and sea ice distribution of the Southern Ocean at the EPILOG Last Glacial Maximum – a circum-Antarctic view based on siliceous microfossil records, Quat. Sci. Rev., 24, 869–896, 2005.

Golledge, N. R., Fogwill, C. J., Mackintosh, A. N., and Buckley, K. M.: Dynamics of the last glacial maximum Antarctic ice-sheet and its
25   response to ocean forcing, Proceedings of the National Academy of Sciences, 109, 16 052–16 056, 2012.

Golledge, N. R., Menviel, L., Carter, L., Fogwill, C. J., England, M. H., Cortese, G., and Levy, R. H.: Antarctic contribution to meltwater pulse 1A from reduced Southern Ocean overturning, Nat. Commun., 5, 5107, 2014.

Golledge, N. R., Keller, E. D., Gomez, N., Naughten, K. A., Bernales, J., Trusel, L. D., and Edwards, T. L.: Global environmental consequences of twenty-first-century ice-sheet melt, Nature, 566, 65–72, 2019.

30   Goosse, H. and Fichefet, T.: Importance of ice-ocean interactions for the global ocean circulation: A model study, J. Geophys. Res., 104, 23 337–23 355, 1999.

Goosse, H., Brovkin, V., Fichefet, T., Haarsma, R., Huybrechts, P., Jongma, J. I., Mouchet, A., Selten, F., Barriat, P.-Y., Campin, J.-M., Deleersnijder, E., Driesschaert, E., Goelzer, H., Janssens, I., Loutre, M.-F., Morales Maqueda, M. A., Opsteegh, T., Mathieu, P.-P., Munhoven, G., Pettersson, E. J., Renssen, H., Roche, D. M., Schaeffer, M., Tartinville, B., Timmermann, A., and Weber, S. L.: Description of the
35   Earth system Model of Intermediate Complexity LOVECLIM version 1.2, Geoscientific Model Development, 3, 603–633, 2010.

He, F., Shakun, J. D., Clark, P. U., Carlson, A. E., Liu, Z., Otto-Bliesner, B. L., and Kutzbach, J. E.: Northern Hemisphere forcing of Southern Hemisphere climate during the last deglaciation, Nature, 494, 81–85, 2013.

Hellmer, H. H., Kauker, F., Timmermann, R., Determann, J., and Rae, J.: Twenty-first-century warming of a large Antarctic ice-shelf cavity by a redirected coastal current, Nature, 485, 225–228, 2012.

Ho, S. L., Mollenhauer, G., Lamy, F., Martínez-Garcia, A., Mohtadi, M., Gersonde, R., Hebbeln, D., Nunez-Ricardo, S., Rosell-Melé, A., and Tiedemann, R.: Sea surface temperature variability in the Pacific sector of the Southern Ocean over the past 700 kyr, Paleoceanography,
5   27, 1–15, 2012.

Holland, P. R., Jenkins, A., and Holland, D. M.: The Response of Ice Shelf Basal Melting to Variations in Ocean Temperature, J. Clim., 21, 2558–2572, 2008.

Huybers, P.: Antarctica's Orbital Beat, Science, 325, 1085–1086, 2009.

Huybers, P. and Denton, G. H.: Antarctic temperature at orbital timescales controlled by local summer duration, Nat. Geosci., 1, 787–792,
10   2008.

Huybrechts, P.: Sea-level changes at the LGM from ice-dynamic reconstructions of the Greenland and Antarctic ice sheets during the glacial cycles, Quat. Sci. Rev., 21, 203–231, 2002.

Huybrechts, P., Gregory, J., Janssens, I., and Wild, M.: Modelling Antarctic and Greenland volume changes during the 20th and 21st centuries forced by GCM time slice integrations, Glob. Planet. Change, 42, 83–105, 2004.

15   IMBIE team: Mass balance of the Antarctic Ice Sheet from 1992 to 2017, Nature, 558, 219–222, 2018.

Jacobs, S. S., Helmer, H. H., Doake, C. S. M., Jenkins, A., and Frolich, R. M.: Melting of ice shelves and the mass balance of Antarctica, J. Glaciol., 38, 375–387, 1992.

Jacobs, S. S., Jenkins, A., Giulivi, C. F., and Dutrieux, P.: Stronger ocean circulation and increased melting under Pine Island Glacier ice shelf, Nat. Geosci., 4, 519–523, 2011.

20   Joughin, I. and Alley, R. B.: Stability of the West Antarctic ice sheet in a warming world, Nat. Geosci., 4, 506–513, 2011.

Joughin, I., Smith, B. E., and Medley, B.: Marine Ice Sheet Collapse Potentially Underway for the Thwaites Glacier Basin, West Antarctica, Science, 735, 2014.

Jouzel, J., Masson-Delmotte, V., Cattani, O., Dreyfus, G., Falourd, S., Hoffmann, G., Minster, B., Nouet, J., Barnola, J.-M., Chappellaz, J., Fischer, H., Gallet, J. C., Johnsen, S. J., Leuenberger, M., Loulergue, L., Luethi, D., Oerter, H., Parrenin, F., Raisbeck, G., Raynaud, D.,
25   Schilt, A., Schwander, J., Selmo, E., Souchez, R., Spahni, R., Stauffer, B., Steffensen, J. P., Stenni, B., Stocker, T. F., Tison, J.-L., Werner, M., and Wolff, E. W.: Orbital and millennial Antarctic climate variability over the past 800,000 years, Science, 317, 793–796, 2007.

Kusahara, K., Sato, T., Oka, A., Obase, T., Greve, R., Abe-Ouchi, A., and Hasumi, H.: Modelling the Antarctic marine cryosphere at the Last Glacial Maximum, Ann. Glaciol., 56, 425–435, 2015.

Laskar, J., Robutel, P., Joutel, F., Gastineau, M., Correia, A. C. M., and Levrard, B.: A long-term numerical solution for the insolation
30   quantities of the Earth, Astron. Astrophys. Suppl. Ser., 428, 261–285, 2004.

Le Brocq, A. M., Payne, A. J., and Vieli, A.: An improved Antarctic dataset for high resolution numerical ice sheet models (ALBMAPv1), Earth System Science Data, 2, 247–260, 2010.

Lisiecki, L. E. and Raymo, M. E.: A Pliocene-Pleistocene stack of 57 globally distributed benthic δ^{18}O records, Paleoceanography, 20, 1–17, 2005.

35   Locarnini, R. A., Mishonov, A. V., Antonov, J. I., Boyer, T. P., Garcia, H. E., Baranova, O. K., Zweng, M. M., and Johnson, D. R.: World Ocean Atlas 2009, Volume 1: Temperature, in: NOAA Atlas NESDIS 68, edited by Levitus, S., U.S. Government Printing Office, 2010.

Lüthi, D., Le Floch, M., Bereiter, B., Blunier, T., Barnola, J.-M., Siegenthaler, U., Raynaud, D., Jouzel, J., Fischer, H., Kawamura, K., and Stocker, T. F.: High-resolution carbon dioxide concentration record 650,000-800,000 years before present, Nature, 453, 379–382, 2008.

Maris, M. N. A., de Boer, B., and Oerlemans, J.: A climate model intercomparison for the Antarctic region: present and past, Clim. Past, 8, 803–814, 2012.

Maris, M. N. A., de Boer, B., Ligtenberg, S. R. M., Crucifix, M., van de Berg, W. J., and Oerlemans, J.: Modelling the evolution of the Antarctic ice sheet since the last interglacial, The Cryosphere, 8, 1347–1360, 2014.

5   Maris, M. N. A., van Wessem, J. M., van de Berg, W. J., de Boer, B., and Oerlemans, J.: A model study of the effect of climate and sea-level change on the evolution of the Antarctic Ice Sheet from the Last Glacial Maximum to 2100, Clim. Dyn., 45, 837–851, 2015.

Martin, M. A., Winkelmann, R., Haseloff, M., Albrecht, T., Bueler, E., Khroulev, C., and Levermann, A.: The Potsdam Parallel Ice Sheet Model (PISM-PIK) – Part 2: Dynamic equilibrium simulation of the Antarctic ice sheet, The Cryosphere, 5, 727–740, 2011.

Medley, B. and Thomas, E. R.: Increased snowfall over the Antarctic Ice Sheet mitigated twentieth-century sea-level rise, Nat. Clim. Chang.,
10   9, 34–39, 2019.

Menviel, L., Timmermann, A., Mouchet, A., and Timm, O. E.: Climate and marine carbon cycle response to changes in the strength of the Southern Hemispheric westerlies, Paleoceanography, 23, 1–10, 2008.

Menviel, L., Timmermann, A., Timm, O. E., and Mouchet, A.: Climate and biogeochemical response to a rapid melting of the West Antarctic Ice Sheet during interglacials and implications for future climate, Paleoceanography, 25, 1–12, 2010.

15   Milankovitch, M.: Kanon der Erdbestrahlung und seine Anwendung auf das Eiszeitenproblem, in: Royal Serbian Academy Special Publication 132, vol. 33, p. 633, Royal Serbian Academy, Belgrade, 1941.

Nick, F. M., Vieli, A., Andersen, M. L., Joughin, I., Payne, A., Edwards, T. L., Pattyn, F., and van de Wal, R. S. W.: Future sea-level rise from Greenland's main outlet glaciers in a warming climate, Nature, 497, 235–238, 2013.

Opsteegh, J. D., Haarsma, R. J., Selten, F. M., and Kattenberg, A.: ECBILT: A dynamic alternative to mixed boundary conditions in ocean
20   models, Tell'Us, 50A, 348–367, 1998.

Parrenin, F., Masson-Delmotte, V., Köhler, P., Raynaud, D., Paillard, D., Schwander, J., Barbante, C., Landais, A., Wegner, A., and Jouzel, J.: Synchronous change of atmospheric CO2 and Antarctic temperature during the last deglacial warming, Science, 339, 1060–1063, 2013.

Petit, J.-R., Jouzel, J., Raynaud, D., Barkov, N. I., Barnola, J.-M., Basile, I., Benders, M., Chappellaz, J., Davis, M., Delaygue, G., Delmotte, M., Kotlyakov, V. M., Legrand, M., Lipenkov, V. Y., Lorius, C., Pépin, L., Ritz, C., Saltzman, E., and Stievenard, M.: Climate and
25   atmospheric history of the past 420,000 years from the Vostok ice core, Antarctica, Nature, 399, 429–436, 1999.

Pollard, D. and DeConto, R. M.: Modelling West Antarctic ice sheet growth and collapse through the past five million years, Nature, 458, 329–332, 2009.

Pollard, D. and DeConto, R. M.: Description of a hybrid ice sheet-shelf model, and application to Antarctica, Geoscientific Model Development, 5, 1273–1295, 2012a.

30   Pollard, D. and DeConto, R. M.: A simple inverse method for the distribution of basal sliding coefficients under ice sheets, applied to Antarctica, The Cryosphere, 6, 953–971, 2012b.

Pollard, D., DeConto, R. M., and Alley, R. B.: Potential Antarctic Ice Sheet retreat driven by hydrofracturing and ice cliff failure, Earth Planet. Sci. Lett., 412, 112–121, 2015.

Pollard, D., Chang, W., Haran, M., Applegate, P., and DeConto, R.: Large ensemble modeling of the last deglacial retreat of the West
35   Antarctic Ice Sheet: comparison of simple and advanced statistical techniques, Geoscientific Model Development, 9, 1697–1723, 2016.

Pritchard, H. D., Ligtenberg, S. R. M., Fricker, H. a., Vaughan, D. G., van den Broeke, M. R., and Padman, L.: Antarctic ice-sheet loss driven by basal melting of ice shelves, Nature, 484, 502–505, 2012.

Raymo, M. E., Lisiecki, L. E., and Nisancioglu, K. H.: Plio-Pleistocene ice volume, Antarctic climate, and the global delta18O record, Science, 313, 492–495, 2006.

Reeh, N.: Parameterization of melt rate and surface temperature on the Greenland ice sheet, Polarforschung, 59, 113–128, 1991.

Ritz, C., Rommelaere, V., and Dumas, C.: Modeling the evolution of Antarctic ice sheet over the last 420,000 years: Implications for altitude

5   changes in the Vostok region, J. Geophys. Res., 106, 31 943–31 964, 2001.

Roche, D. M., Dokken, T. M., Goosse, H., Renssen, H., and Weber, S. L.: Climate of the Last Glacial Maximum: sensitivity studies and model-data comparison with the LOVECLIM coupled model, Clim. Past, 3, 205–224, 2007.

Roche, D. M., Crosta, X., and Renssen, H.: Evaluating Southern Ocean sea-ice for the Last Glacial Maximum and pre-industrial climates: PMIP-2 models and data evidence, Quat. Sci. Rev., 56, 99–106, 2012.

10   Scambos, T. A., Bell, R. E., Alley, R. B., Anandakrishnan, S., Bromwich, D. H., Brunt, K., Christianson, K., Creyts, T., Das, S. B., DeConto, R., Dutrieux, P., Fricker, H. A., Holland, D., MacGregor, J., Medley, B., Nicolas, J. P., Pollard, D., Siegfried, M. R., Smith, A. M., Steig, E. J., Trusel, L. D., Vaughan, D. G., and Yager, P. L.: How much, how fast?: A science review and outlook for research on the instability of Antarctica's Thwaites Glacier in the 21st century, Glob. Planet. Change, 153, 16–34, 2017.

Schoof, C.: Ice sheet grounding line dynamics: Steady states, stability, and hysteresis, Journal of Geophysical Research: Earth Surface, 112,

15   1–19, 2007.

Shackleton, N. J.: The 100,000-year ice-age cycle identified and found to lag temperature, carbon dioxide and orbital eccentricity, Science, 289, 1897–1902, 2000.

Spratt, R. M. and Lisiecki, L. E.: A Late Pleistocene sea level stack, Clim. Past, 12, 1079–1092, 2016.

Stap, L. B., van de Wal, R. S. W., de Boer, B., Bintanja, R., and Lourens, L. J.: Interaction of ice sheets and climate during the past 800 000

20   years, Clim. Past, 10, 2135–2152, 2014.

Steig, E. J., Morse, D. L., Waddington, E. D., Stuiver, M., Grootes, P. M., Mayewski, P. A., Twickler, M. S., and Whitlow, S. I.: Wisconsinan and Holocene climate history from an ice core at Taylor Dome, Western Ross Embayment, Antarctica, Geogr. Ann., 82A, 213–235, 2000.

Steig, E. J., Ding, Q., Battisti, D. S., and Jenkins, A.: Tropical forcing of Circumpolar Deep Water Inflow and outlet glacier thinning in the Amundsen Sea Embayment, West Antarctica, Ann. Glaciol., 53, 19–28, 2012.

25   Steig, E. J., Huybers, K., Singh, H. A., Steiger, N. J., Ding, Q., Frierson, D. M. W., Popp, T., and White, J. W. C.: Influence of West Antarctic Ice Sheet collapse on Antarctic surface climate, Geophys. Res. Lett., 42, 2015GL063 861, 2015.

Thoma, M., Jenkins, A., Holland, D. M., and Jacobs, S. S.: Modelling Circumpolar Deep Water intrusions on the Amundsen Sea continental shelf, Antarctica, Geophys. Res. Lett., 35, L18 602, 2008.

Tigchelaar, M., Timmermann, A., Pollard, D., Friedrich, T., and Heinemann, M.: Local insolation changes enhance Antarctic interglacials:

30   Insights from an 800,000-year ice sheet simulation with transient climate forcing, Earth Planet. Sci. Lett., 495, 69–78, 2018.

Timm, O. E. and Timmermann, A.: Simulation of the last 21,000 years using accelerated transient boundary conditions, J. Clim., 20, 4377–4401, 2007.

Timmermann, A. and Friedrich, T.: Late Pleistocene climate drivers of early human migration, Nature, 538, 92–95, 2016.

Timmermann, A., Timm, O. E., Stott, L., and Menviel, L.: The roles of CO_2 and orbital forcing in driving Southern Hemispheric temperature

35   variations during the last 21000 yr, J. Clim., 22, 1626–1640, 2009.

Timmermann, A., Friedrich, T., Timm, O. E., Chikamoto, M. O., Abe-Ouchi, A., and Ganopolski, A.: Modeling obliquity and CO2 effects on Southern Hemisphere climate during the past 408 ka, J. Clim., 27, 1863–1875, 2014.

Vallelonga, P., Barbante, C., Cozzi, G., Gabrieli, J., Schüpbach, S., Spolaor, A., and Turetta, C.: Iron fluxes to Talos Dome, Antarctica, over the past 200 kyr, Clim. Past, 9, 597–604, 2013.

van de Berg, W. J., van den Broeke, M. R., Reijmer, C. H., and van Meijgaard, E.: Reassessment of the Antarctic surface mass balance using calibrated output of a regional atmospheric climate model, J. Geophys. Res. D: Atmos., 111, 1–15, 2006.

5   van den Broeke, M.: Strong surface melting preceded collapse of Antarctic Peninsula ice shelf, Geophys. Res. Lett., 32, 1–4, 2005.

Weber, M. E., Clark, P. U., Kuhn, G., Timmermann, A., Sprenk, D., Gladstone, R., Zhang, X., Lohmann, G., Menviel, L., Chikamoto, M. O., Friedrich, T., and Ohlwein, C.: Millennial-scale variability in Antarctic ice-sheet discharge during the last deglaciation, Nature, 2014.
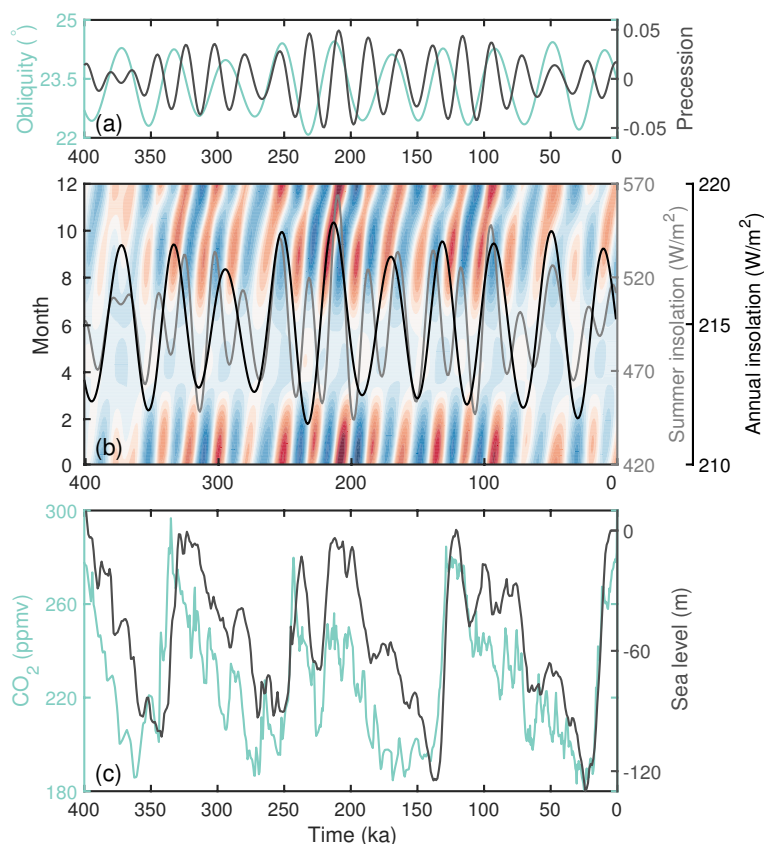
Figure 1. Climate drivers over the last 400 ka – (a) precession (grey) and obliquity (teal) (Laskar et al., 2004); (b) monthly insolation anomalies (colors, contours ranging from $\pm 65\ \mathrm{W\,m^{-2}}$), annual mean insolation (black) and summer insolation (grey) at 65 °S as a result of the orbital forcing in (a) (Laskar et al., 2004); (c) atmospheric CO_2 concentration (teal; Lüthi et al., 2008) and global sea level (m) (grey; Spratt and Lisiecki, 2016).

The Cryosphere
Discussions

Open Access

EGU
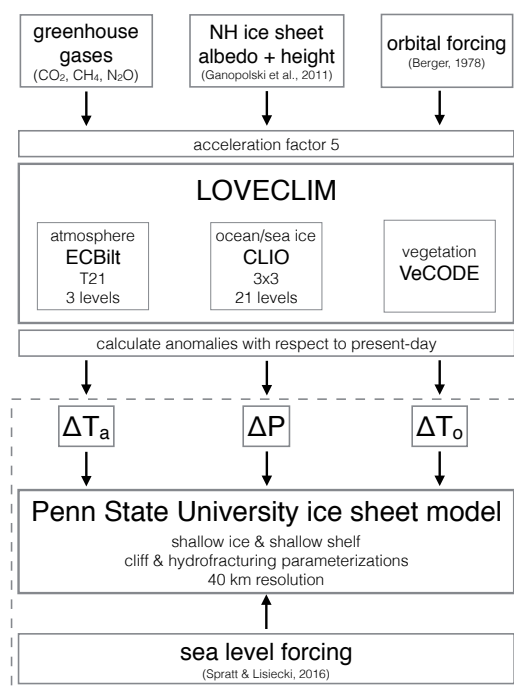
Figure 2. Schematic illustrating the modeling setup as described in Sect. 2.
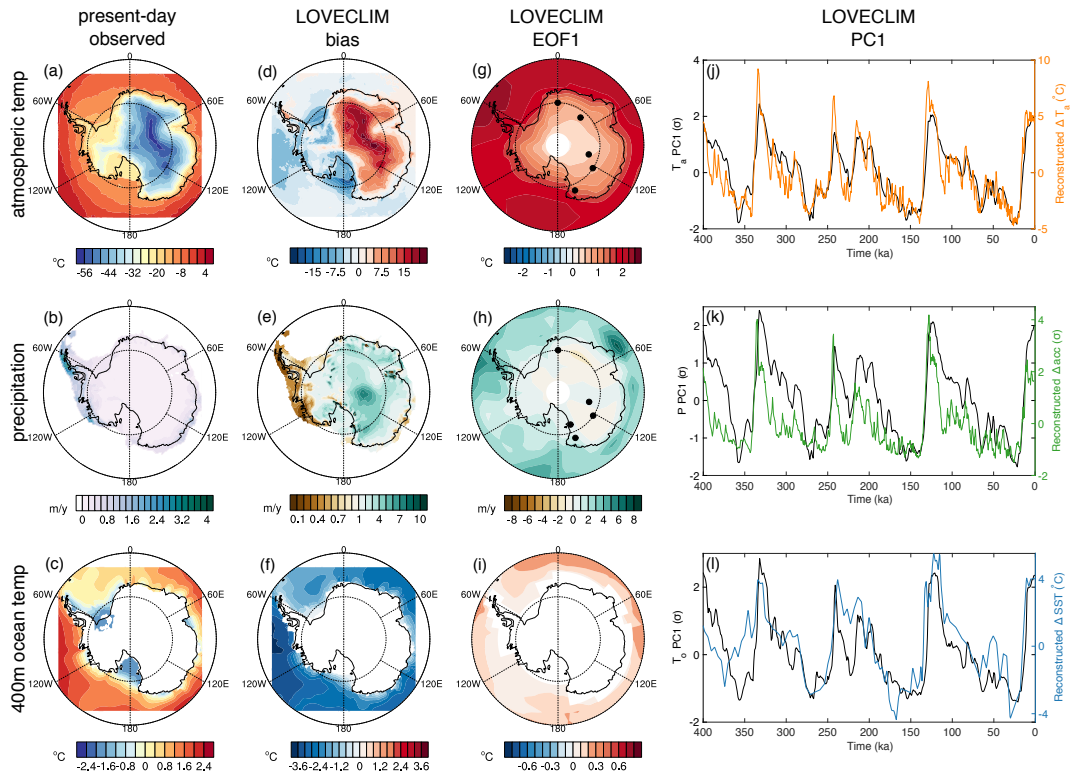
Figure 3. Climate forcing on the ice model grid – (left) Present-day climate conditions (Locarnini et al., 2010; Le Brocq et al., 2010), (second from left) LOVECLIM bias with respect to present-day climate, (third from left) first EOF and (right) first PC1 in LOVECLIM for (top) annual mean atmospheric temperature, (middle) annual mean accumulation (observed) and precipitation (LOVECLIM) and (bottom) annual mean ocean temperature at 400 m depth. For annual mean temperature the LOVECLIM temperatures were first adjusted to observed elevations (Le Brocq et al., 2010) using a lapse-rate correction of 0.008 °C m^{-1}. The atmospheric and ocean temperature biases are plotted as LOVECLIM–observed, while the precipitation bias is plotted as LOVECLIM/observed. In addition, (j) shows a composite of reconstructed temperature anomalies from ice cores (°C, orange; locations indicated by black dots in (g); Parrenin et al., 2013), (k) shows a composite of reconstructed accumulation anomalies from ice cores (σ, green; locations indicated by black dots in (h); Steig et al., 2000; Bazin et al., 2013; Vallelonga et al., 2013) and (l) shows reconstructed SST anomalies at 80 °W, 54 °S (°C, blue; Ho et al., 2012).
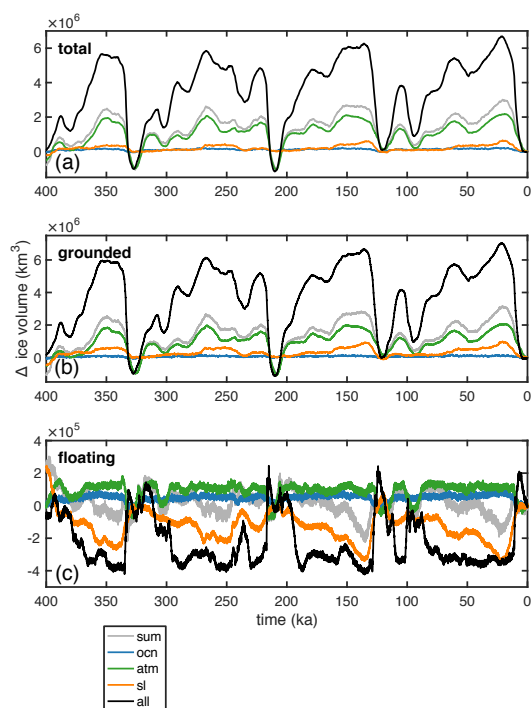
Figure 4. Ice sheet evolution over the last 400 ka for experiments 'ocn' (blue), 'atm' (green), 'sl' (orange), and 'all' (black) (Table 1) – (a) total ice sheet volume; (b) grounded ice sheet volume; and (c) floating ice sheet volume. The grey line is the sum of the individual runs 'ocn', 'atm', and 'sl'.
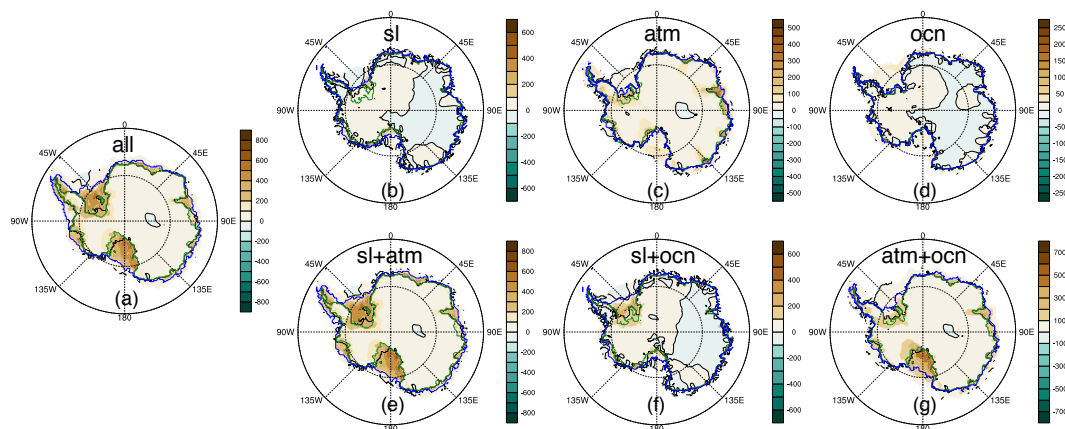
Figure 5. Dominant spatial pattern (first EOF) of ice sheet thickness variability (m) and minimum (green), maximum (blue) and present-day (black) grounding line extent for (a) 'all', minimum at 331 ka, maximum at 18 ka, 75.8% of variance explained; (b) 'sl', minimum at 121 ka, maximum at 18 ka, 39.4% of variance explained; (c) 'atm', minimum at 331 ka, maximum at 350 ka, 50.7% of variance explained; (d) 'ocn', minimum at 7 ka, maximum at 156 ka, 9.6% of variance explained; (e) 'sl+atm', minimum at 331 ka, maximum at 20 ka, 76.6% of variance explained; (f) 'sl+ocn', minimum at 122 ka, maximum at 140 ka, 50.5% of variance explained; (g) 'atm+ocn', minimum at 330 ka, maximum at 354 ka, 63.1% of variance explained.
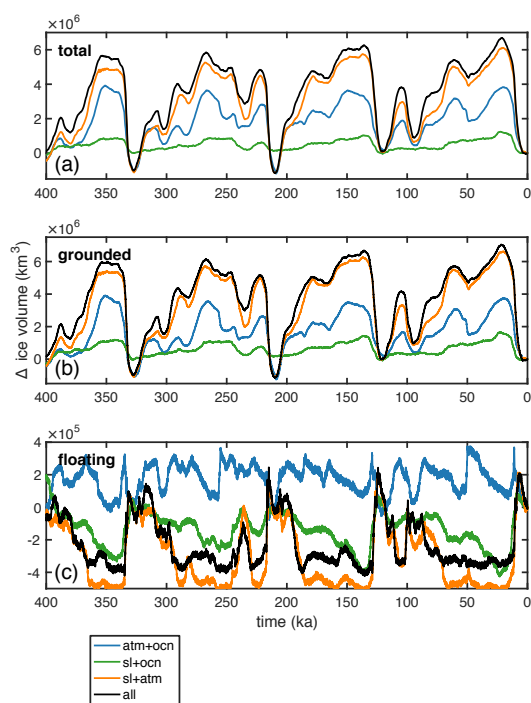
Figure 6. Ice sheet evolution over the last 400 ka for experiments 'atm+ocn' (blue), 'sl+ocn' (green), 'sl+atm' (orange), and 'all' (black) (Table 1) – (a) total ice sheet volume; (b) grounded ice sheet volume; and (c) floating ice sheet volume.
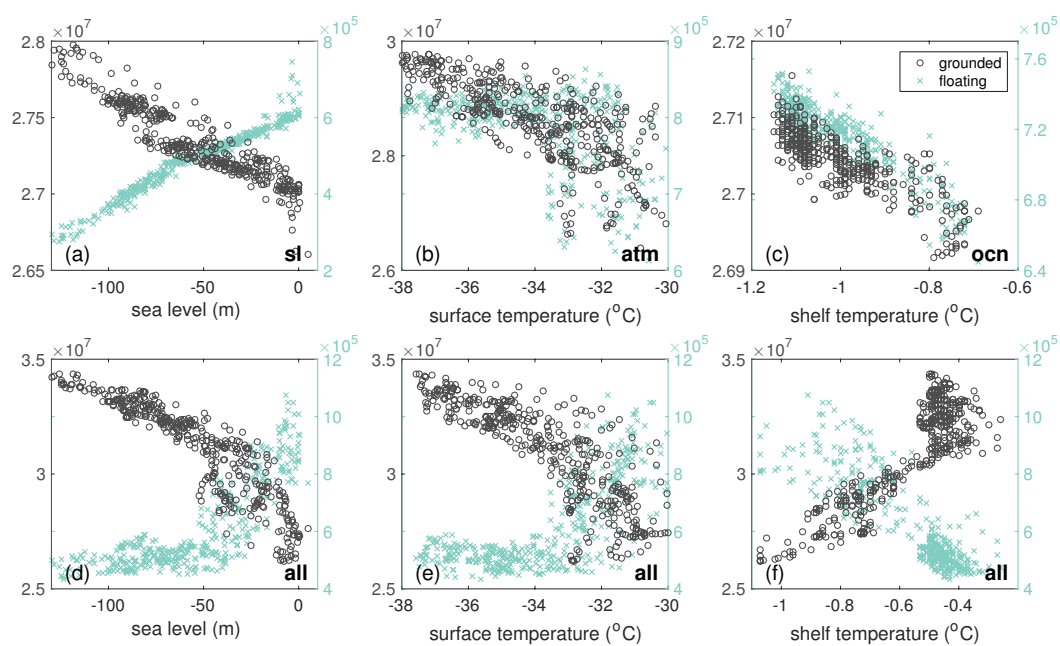
Figure 7. Ice sheet averaged forcing terms against floating (teal crosses) and grounded (grey circles) ice volume (km^3) – sea level in (a) 'sl' and (d) 'all'; atmospheric surface temperature in (b) 'atm' and (e) 'all'; and temperature beneath the ice shelves in (c) 'ocn' and (f) 'all'.
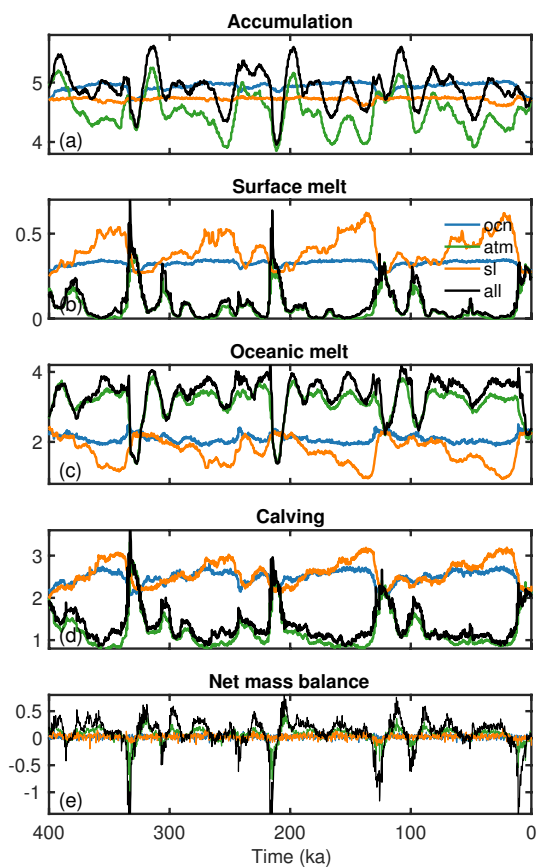
Figure 8. Ice sheet integrated mass balance terms ($10^3\,\mathrm{Gt\,y^{-1}}$) for experiments 'ocn' (blue), 'atm' (green), 'sl' (orange) and 'all' (black) – (a) accumulation, (b) surface melt, (c) oceanic melt, (d) calving, and (e) net mass balance.

The Cryosphere
Discussions

Table 1. Overview of the sensitivity experiments described in Sect. 2.2.3

experiment	description
all	all forcings (Eqs. (1), (2), (3) & Spratt and Lisiecki (2016))
atm	only atmospheric forcing (Eqs. (1) & (2))
ocn	only ocean temperature forcing (Eq. (3))
sl	only sea level forcing (Spratt and Lisiecki (2016))
sl+atm	sea level and atmospheric forcing (Eqs. (1), (2) & Spratt and Lisiecki (2016))
sl+ocn	sea level and ocean temperature forcing (Eqs. (3) & Spratt and Lisiecki (2016))
atm+ocn	atmospheric and ocean temperature forcing (Eqs. (1), (2), (3))